Supplementary Information for

Zinc-Induced Ordering in $L1_0$-Type Platinum-Based Nanoalloys for the Electrocatalytic Oxygen Reduction Reaction

Wu Tian,[a] Ryota Sato,[*b] Tomoki Uchiyama,[c] Yasutomi Tatetsu,[d] Kenshi Matsumoto,[b] Yoshiharu Uchimoto,[c] and Toshiharu Teranishi[*ab]

[a] Department of Chemistry, Kyoto University, Uji, Kyoto 611-0011, Japan.
[b] Institute for Chemical Research, Kyoto University, Uji, Kyoto 611-0011, Japan.
[c] Graduate School of Human and Environmental Studies, Kyoto University, Sakyo-ku, Kyoto 606-8501, Japan.
[d] Department of Health Informatics, Meio University, Biimata, Nago, Okinawa 905-8585, Japan.

*Corresponding Authors: Ryota Sato: r-sato@scl.kyoto-u.ac.jp; Toshiharu Teranishi: teranisi@scl.kyoto-u.ac.jp

Table of Contents

Supplementary Figures:

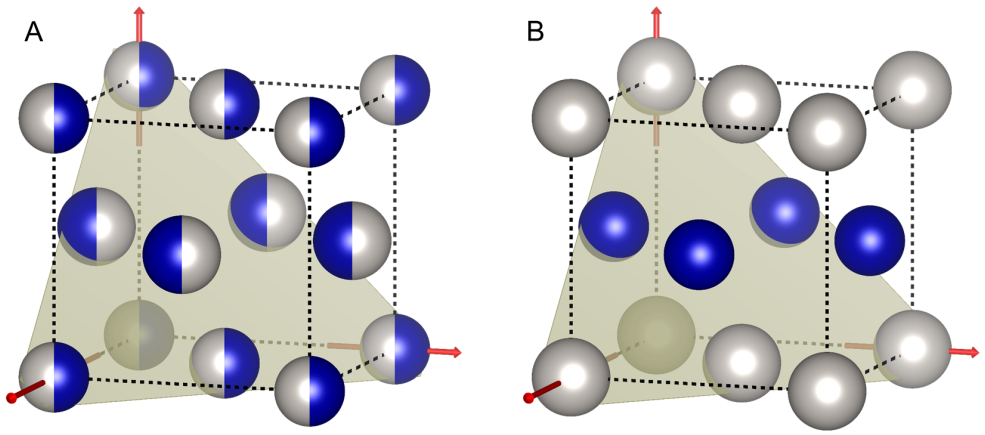

Figure S1. Unit cells of (A) *A*1-Pt*M* and (B) $L1_0$-Pt*M* alloys. The (111) planes are indicated by gray triangles.

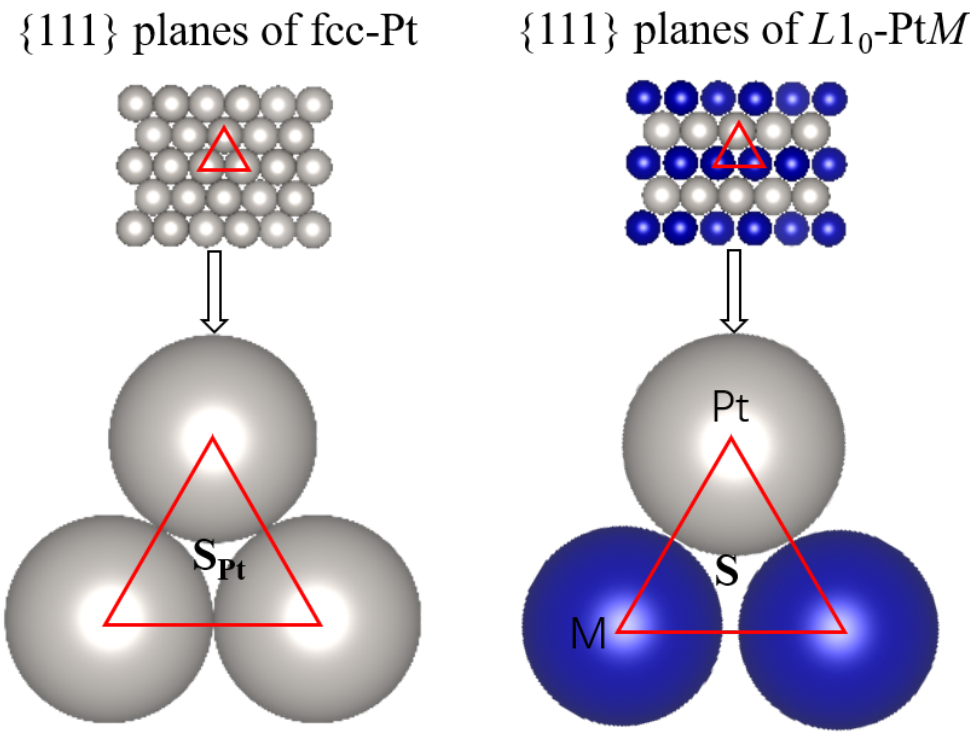

$$Strain(\%) = \frac{S - S_{Pt}}{S_{Pt}} \quad (1)$$

Figure S2. Schematic diagrams used for the calculation of surface strain.[2]

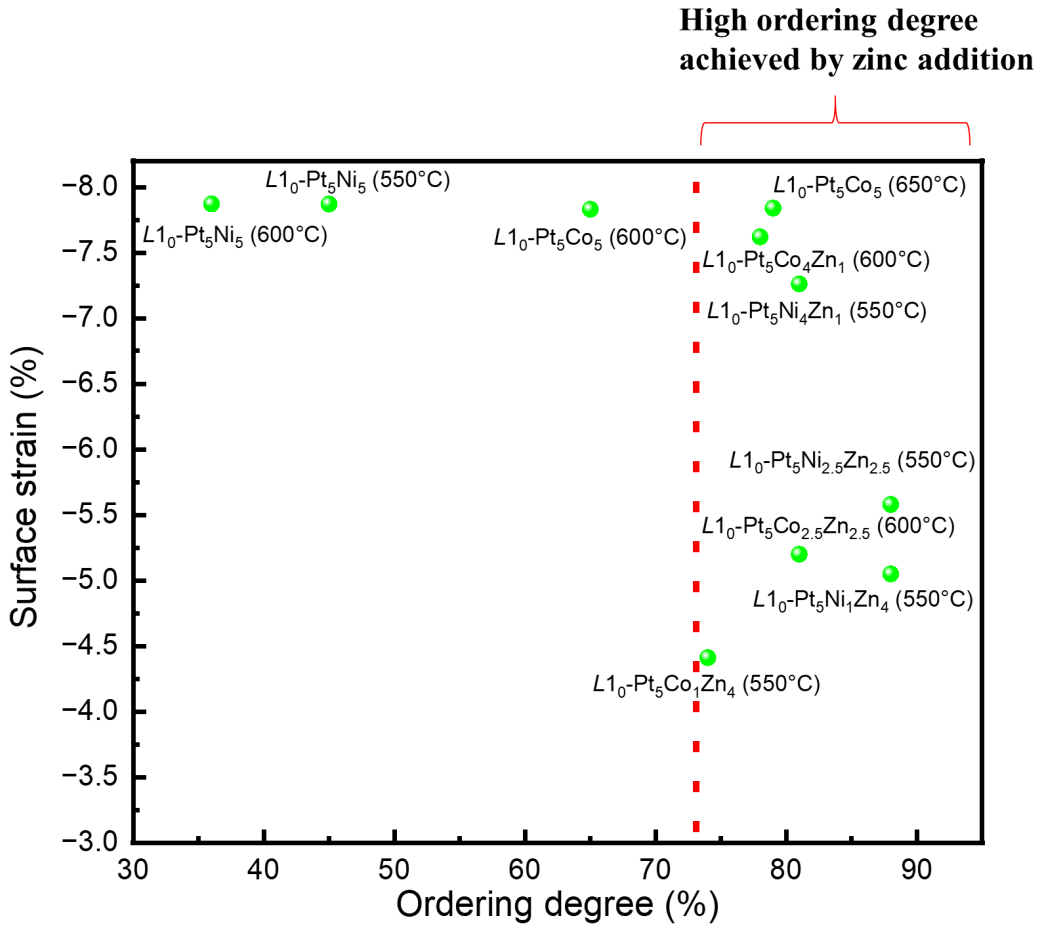

Figure S3. Dependence of the surface strain of Pt shells on the ordering degree of $L1_0$ cores.

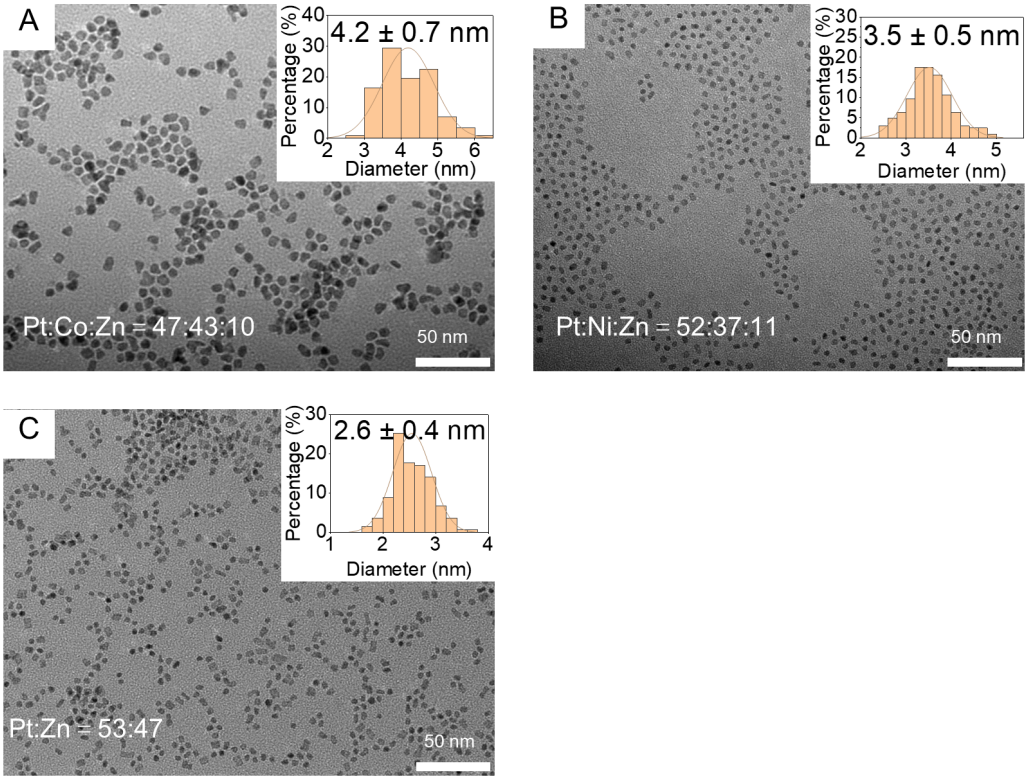

Figure S4. TEM images and size distributions (inset) of as-synthesized (A) $Pt_5Co_1Zn_4$, (B) $Pt_5Ni_1Zn_4$ and (C) Pt_5Zn_5 NPs.

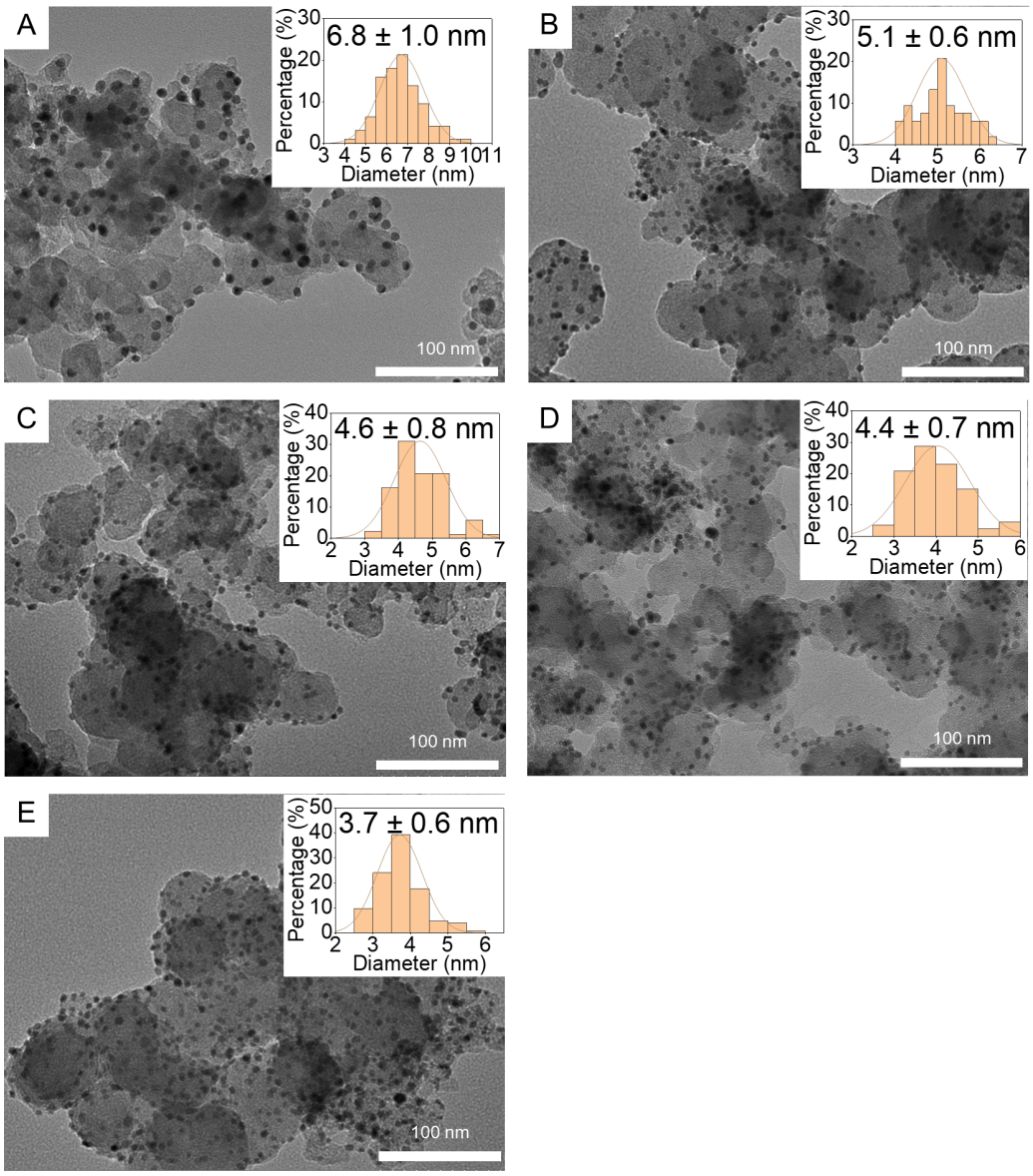

Figure S5. TEM images and size distributions (inset) of carbon-loaded (A) $L1_0$-PtCo-600 °C, (B) $L1_0$-$Pt_5Co_4Zn_1$-600 °C, (C) $L1_0$-$Pt_5Co_{2.5}Zn_{2.5}$-600 °C, (D) $L1_0$-$Pt_5Co_1Zn_4$-550 °C and (E) $L1_0$-Pt_5Zn_5-550 °C NPs.

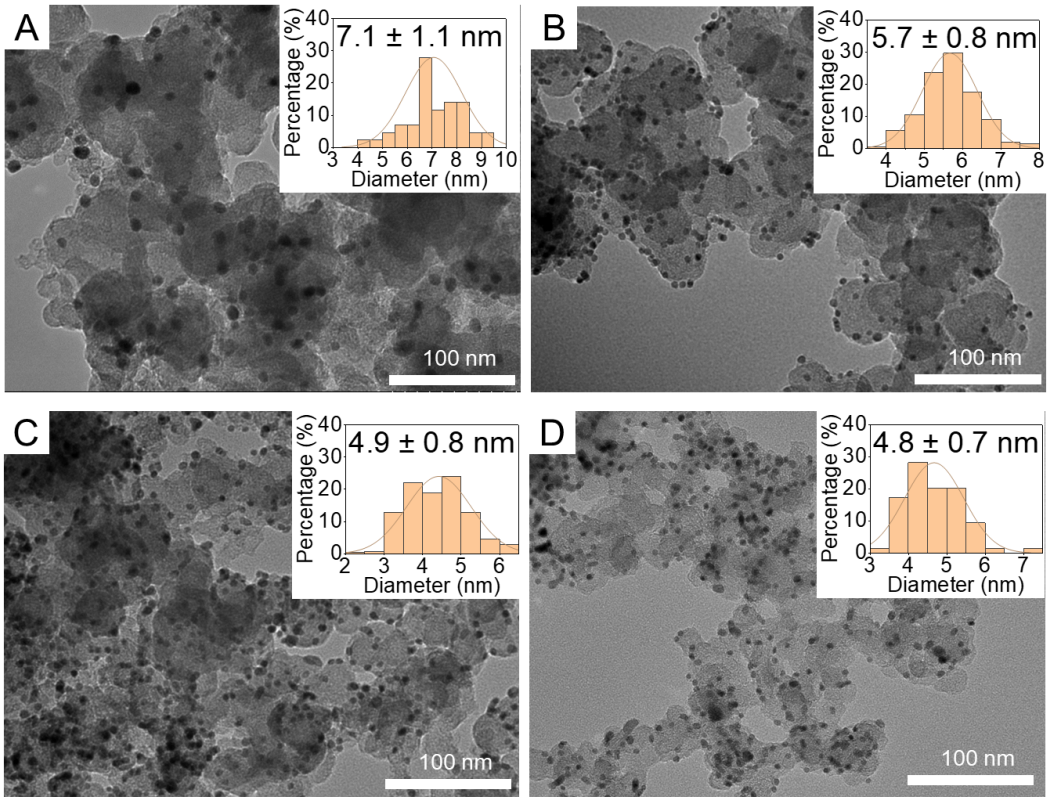

Figure S6. TEM images and size distributions (inset) of carbon-loaded (A) $L1_0$-PtNi-550 °C, (B) $L1_0$-$Pt_5Ni_4Zn_1$-550 °C, (C) $L1_0$-$Pt_5Ni_{2.5}Zn_{2.5}$-550 °C and (D) $L1_0$-$Pt_5Ni_1Zn_4$-550 °C NPs.

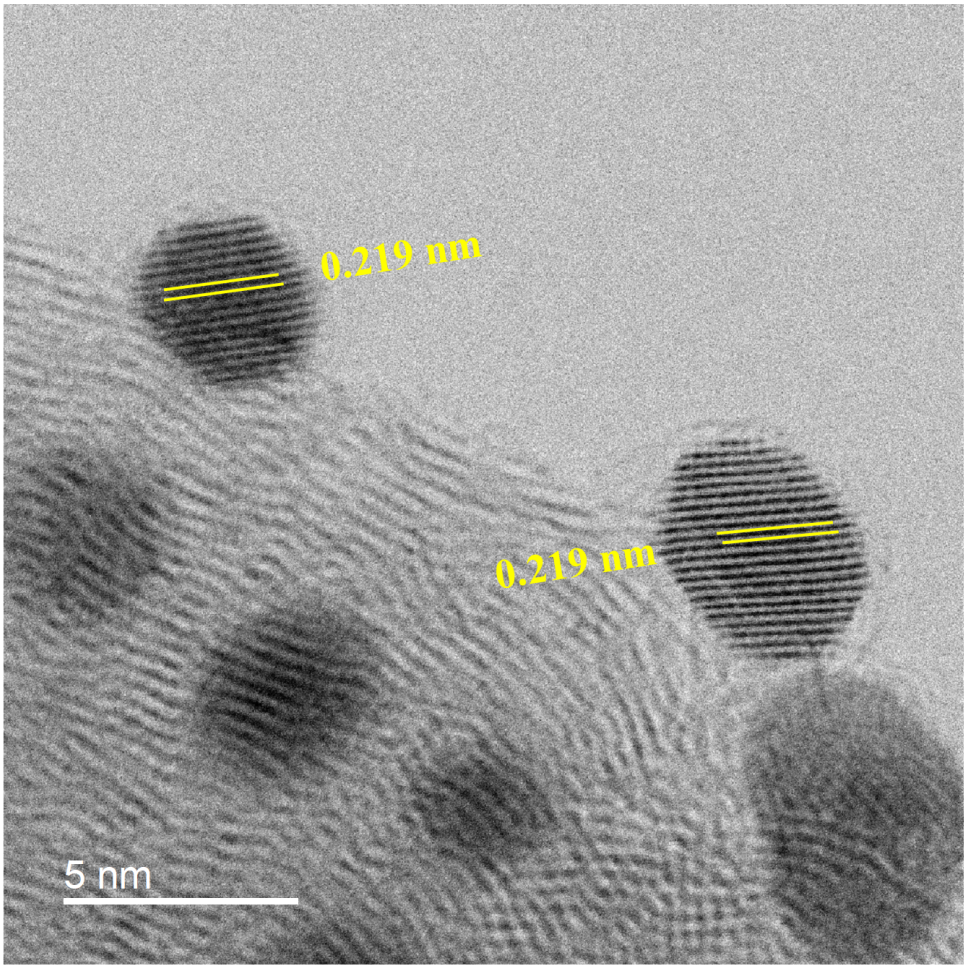

Figure S7. HR-TEM image of $L1_0$-$Pt_5Co_{2.5}Zn_{2.5}$@Pt NPs supported on carbon after reductive annealing and subsequent acid treatment. The lattice spacing is 0.219 nm, which is between those of $L1_0$-PtCo ($d_{(111)}$ = 0.217 nm) and $L1_0$-PtZn ($d_{(111)}$ = 0.222 nm), indicating the formation of $L1_0$-Pt(Co,Zn) structure.

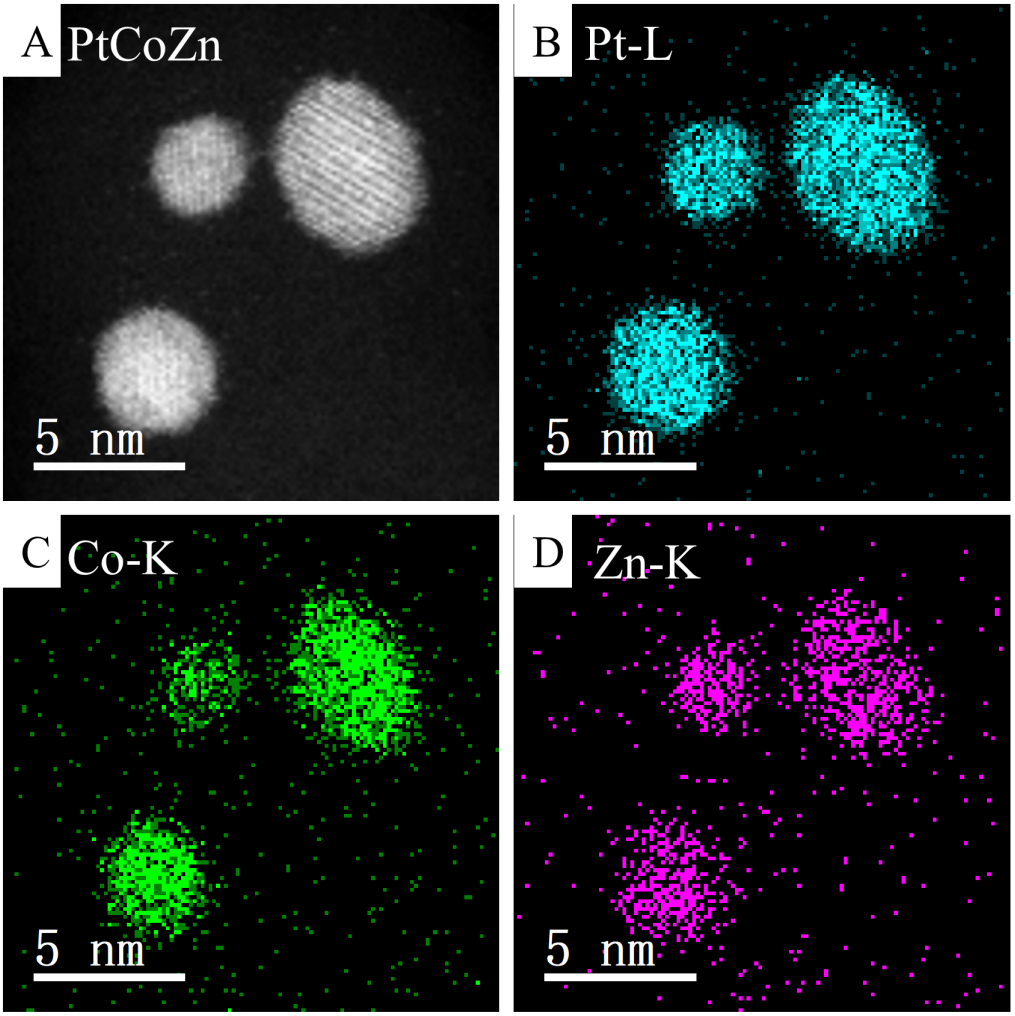

Figure S8. (A) STEM image and corresponding (B) Pt-L, (C) Co-K and (D) Zn-K elemental mapping images of $L1_0$-$Pt_5Co_{2.5}Zn_{2.5}$@Pt NPs.

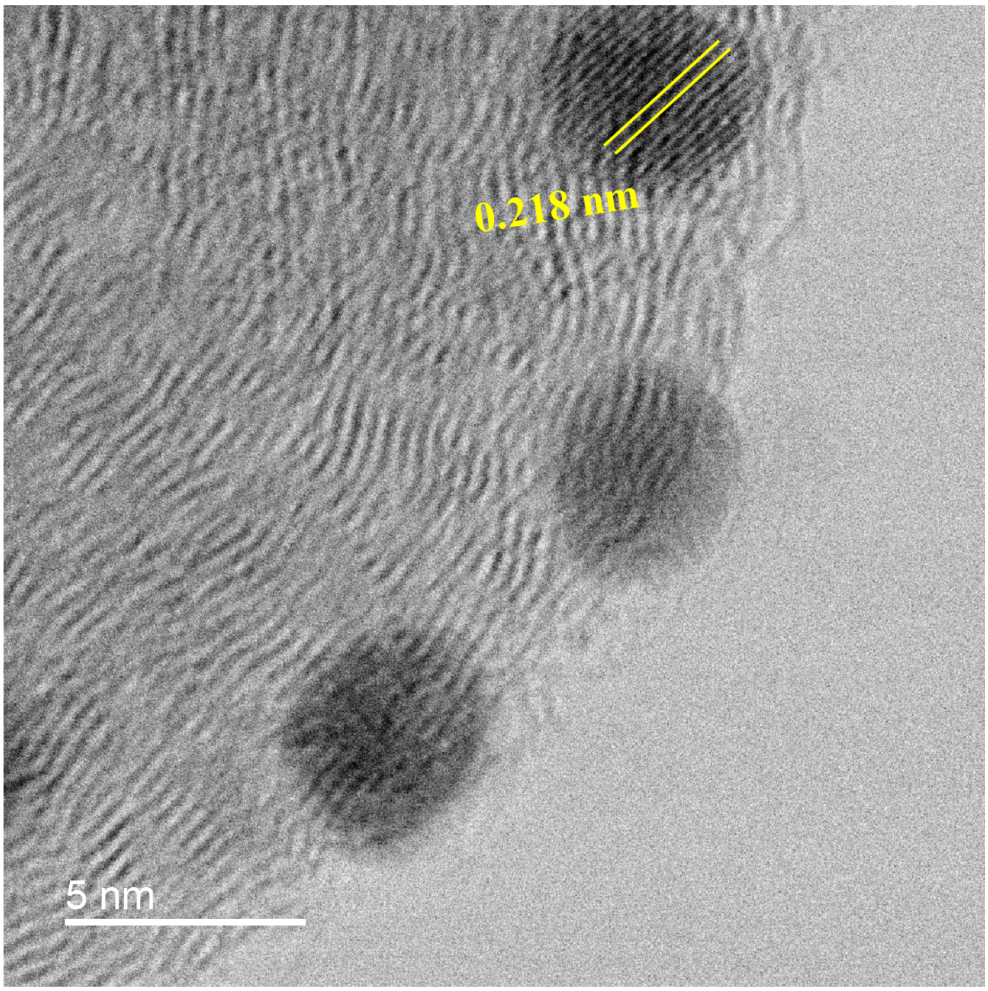

Figure S9. HR-TEM image of $L1_0$-$Pt_5Ni_{2.5}Zn_{2.5}$ NPs supported on carbon after reductive annealing without subsequent acid treatment. The lattice spacing is 0.218 nm which is between those of $L1_0$-PtNi ($d_{(111)}$ = 0.217 nm) and $L1_0$-PtZn ($d_{(111)}$ = 0.222 nm), indicating the formation of $L1_0$-Pt(Ni,Zn) structure.

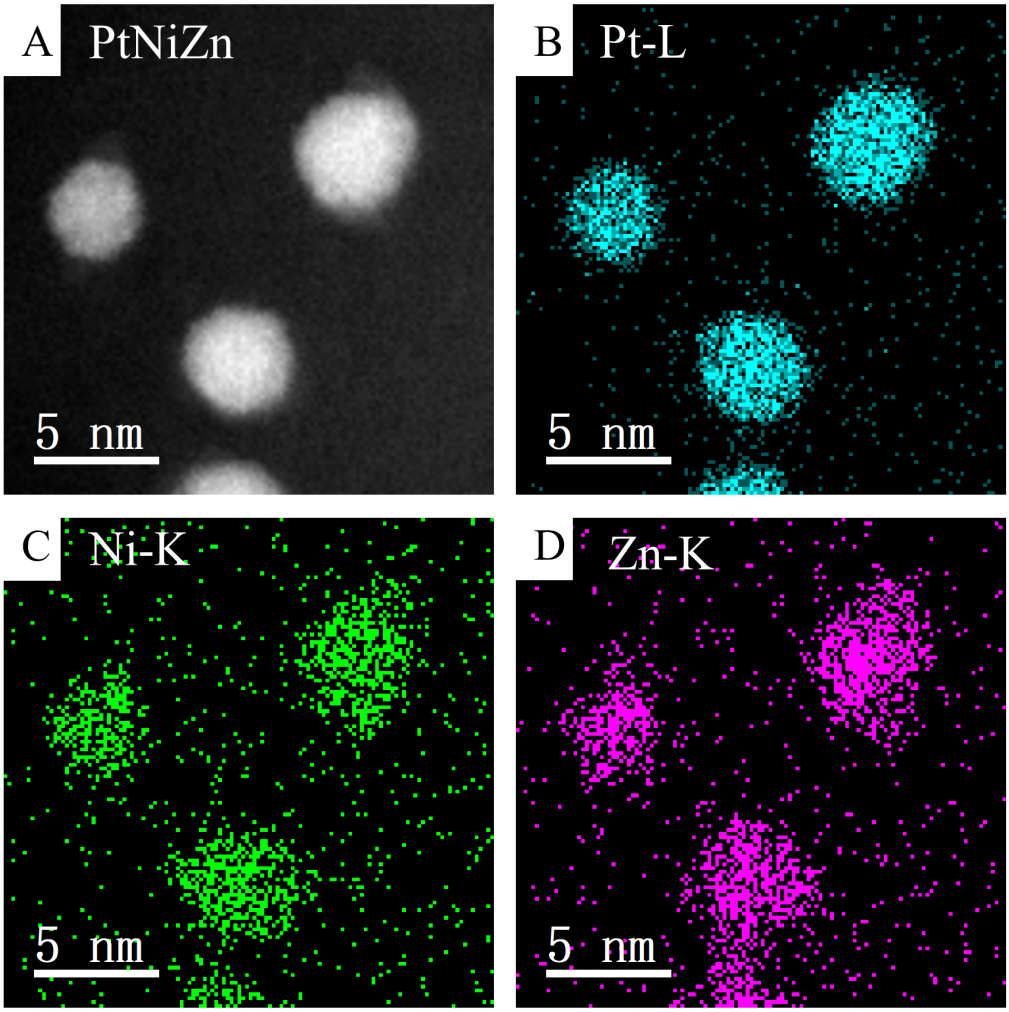

Figure S10. (A) STEM image and corresponding (B) Pt-L, (C) Ni-K and (D) Zn-K elemental mapping images of $L1_0$-$Pt_5Ni_{2.5}Zn_{2.5}$ NPs.

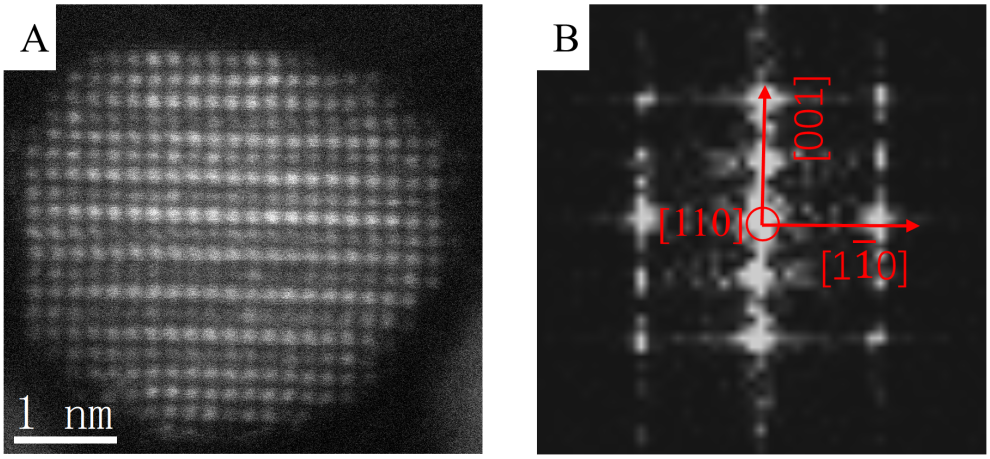

Figure S11. (A) HAADF-STEM image and (B) fast Fourier transform (FFT) image of an $L1_0$-$Pt_5Ni_{2.5}Zn_{2.5}$ NP (zone axis is the <110> direction). Alternative columns of bright dots (Pt) and gray dots (Ni, Zn) correspond to $L1_0$ structure. Superlattice spots corresponding to $L1_0$ also appear in the FFT image.

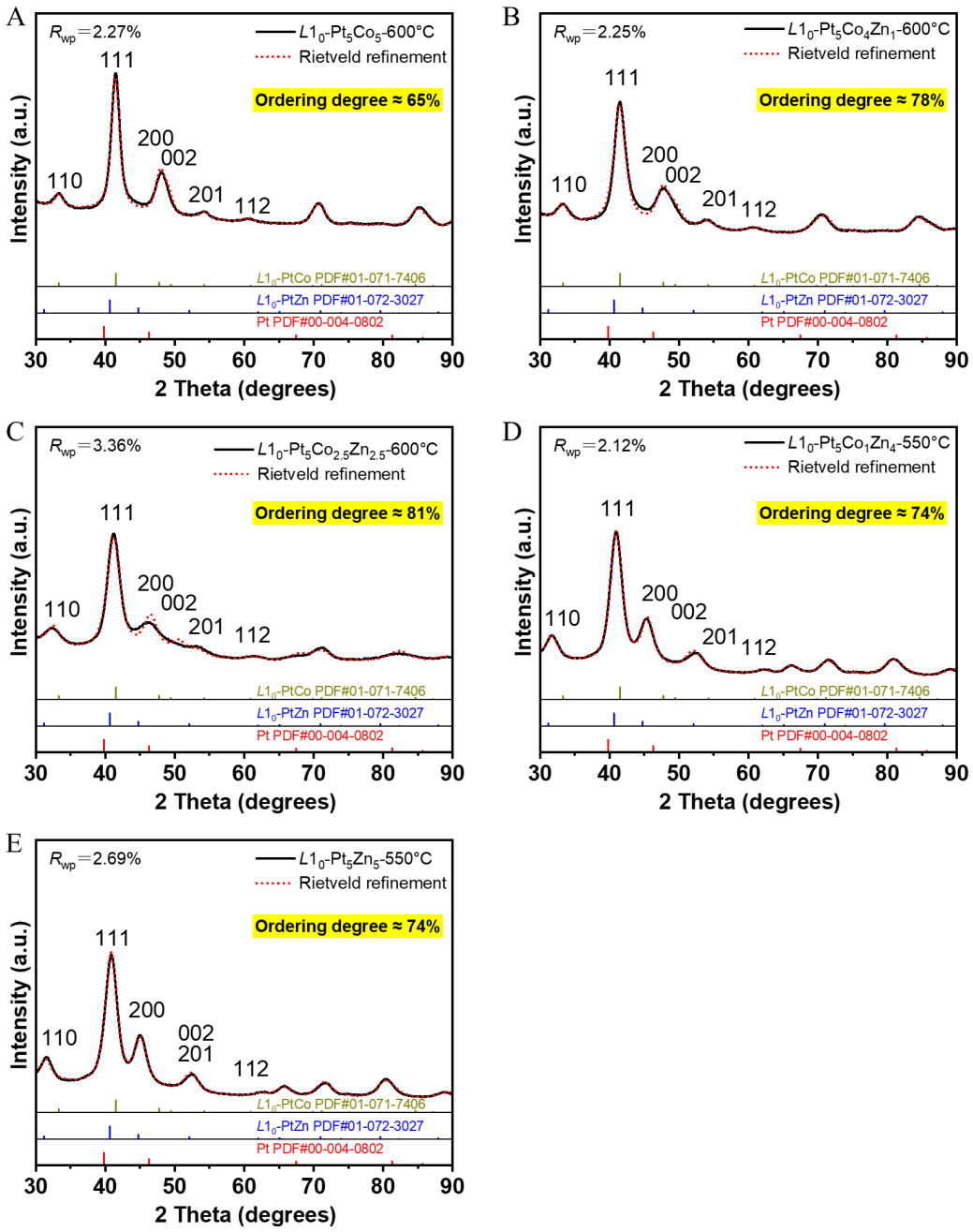

Figure S12. Rietveld refinement of XRD patterns of (A) $L1_0$-Pt_5Co_5, (B) $L1_0$-$Pt_5Co_4Zn_1$, (C) $L1_0$-$Pt_5Co_{2.5}Zn_{2.5}$, (D) $L1_0$-$Pt_5Co_1Zn_4$ and (E) $L1_0$-Pt_5Zn_5 NPs obtained by reductive annealing for 6 h. The $L1_0$-ordering degree was evaluated by calculating the intensity ratio I_{110}/I_{111}.

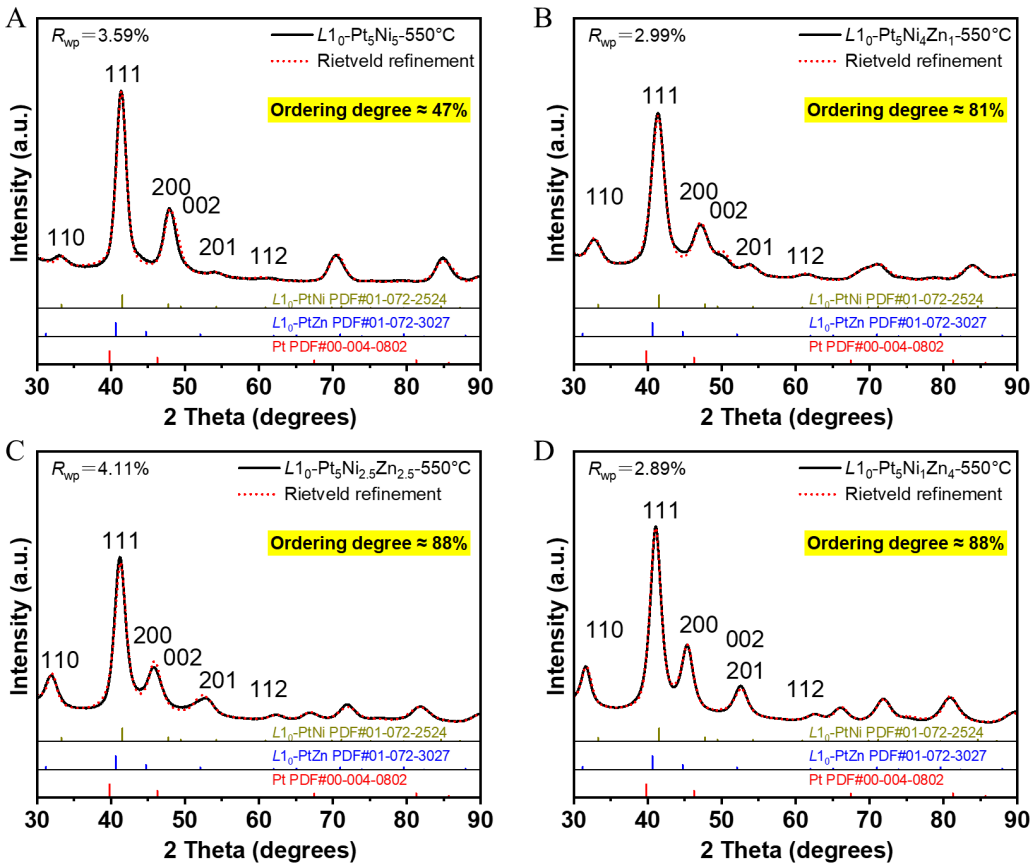

Figure S13. Rietveld refinement of XRD patterns of (A) $L1_0$-Pt_5Ni_5, (B) $L1_0$-$Pt_5Ni_4Zn_1$, (C) $L1_0$-$Pt_5Ni_{2.5}Zn_{2.5}$ and (D) $L1_0$-$Pt_5Ni_1Zn_4$ NPs obtained by reductive annealing at 550 °C for 6 h. The $L1_0$-ordering degree was evaluated by calculating the intensity ratio I_{110}/I_{111}.

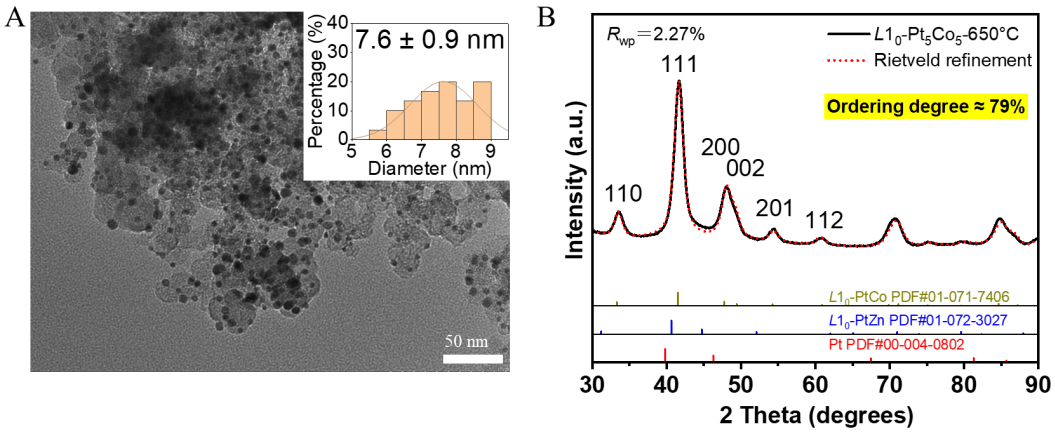

Figure S14. (A) TEM image and size distribution (inset) of 7.6-nm $L1_0$-Pt_5Co_5 NPs supported on carbon. (B) Rietveld refinement of the XRD pattern of $L1_0$-Pt_5Co_5 NPs obtained by reductive annealing at 650 °C for 6 h. The $L1_0$-ordering degree was evaluated by calculating the intensity ratio I_{110}/I_{111}.

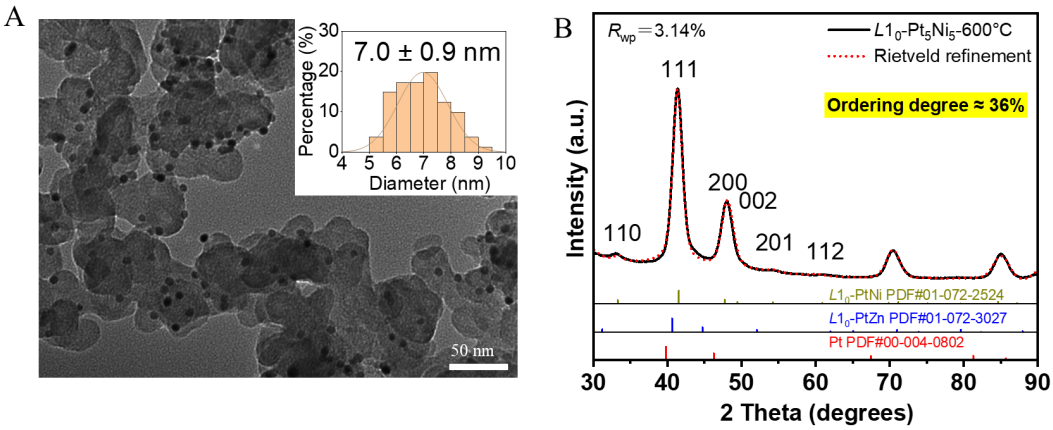

Figure S15. (A) TEM image and size distribution (inset) of 6.8-nm $L1_0$-Pt_5Ni_5 NPs supported on carbon. (B) Rietveld refinement of the XRD pattern of $L1_0$-Pt_5Ni_5 NPs obtained by reductive annealing at 600 °C for 6 h. The $L1_0$-ordering degree was evaluated by calculating the intensity ratio I_{110}/I_{111}.

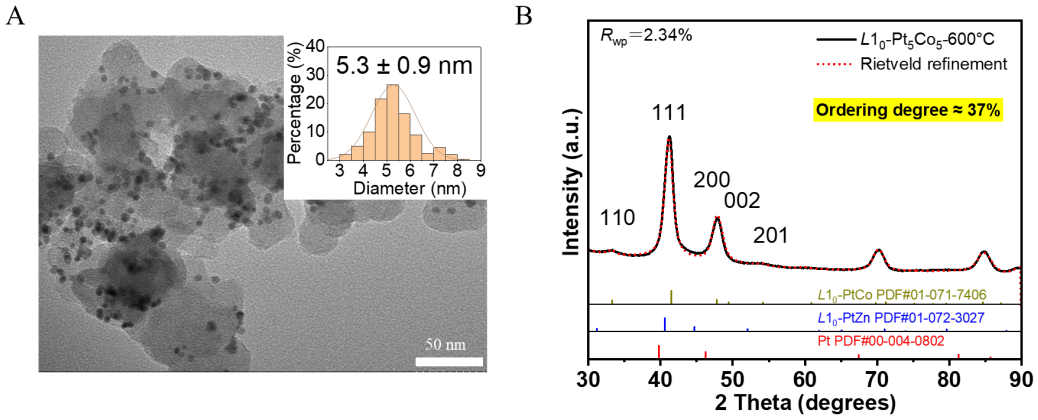

Figure S16. (A) TEM image and size distribution (inset) of 5.3-nm $L1_0$-Pt_5Ni_5 NPs supported on carbon. (B) Rietveld refinement of the XRD pattern of 5.3-nm $L1_0$-Pt_5Co_5 NPs obtained by reductive annealing at 600 °C for 6 h. The $L1_0$-ordering degree was evaluated by calculating the intensity ratio I_{110}/I_{111}.

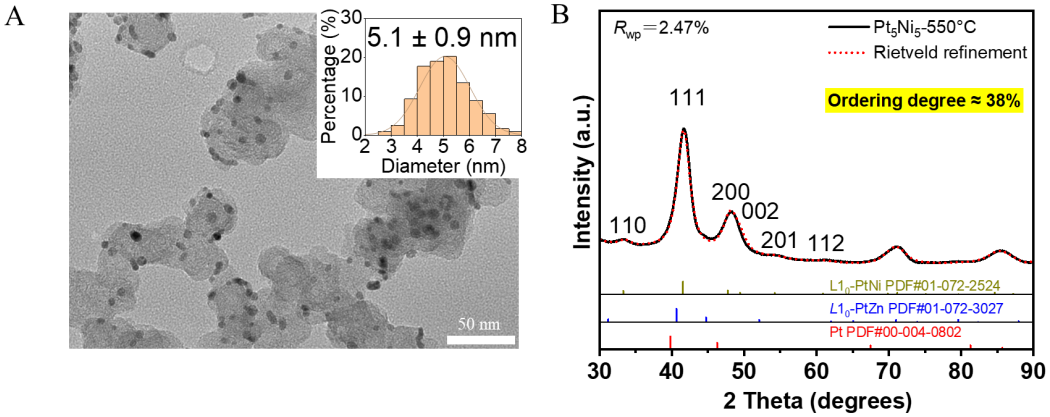

Figure S17. (A) TEM image and size distribution (inset) of 5.1-nm $L1_0$-Pt_5Ni_5 NPs supported on carbon. (B) Rietveld refinement of the XRD pattern of 5.1-nm $L1_0$-Pt_5Ni_5 NPs obtained by reductive annealing at 550 °C for 6 h. The $L1_0$-ordering degree was evaluated by calculating the intensity ratio I_{110}/I_{111}.

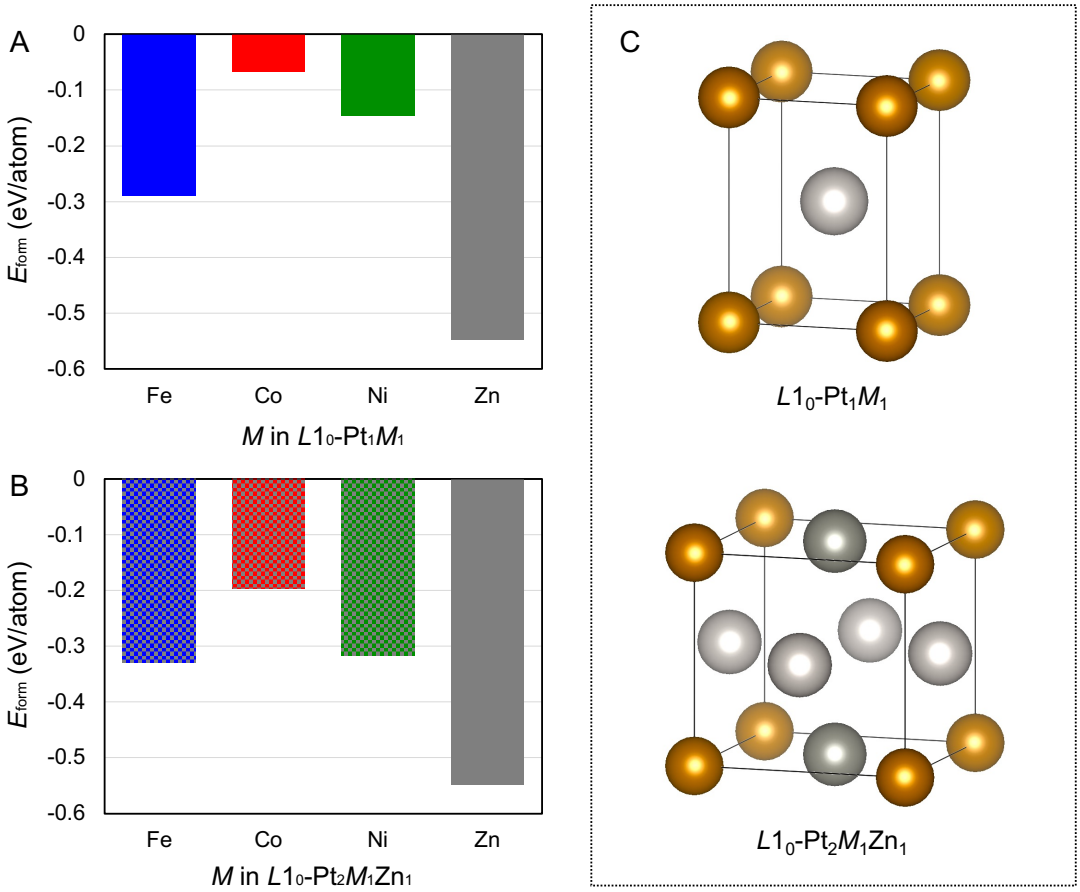

Figure S18. Formation energies (E_{form}) of (A) $L1_0$-Pt_1M_1 and (B) $L1_0$-$Pt_2M_1Zn_1$ calculated using the OpenMX code. (C) Atomic models of $L1_0$-Pt_1M_1 (upper) and $L1_0$-$Pt_2M_1Zn_1$ (lower) used for DFT calculations, where the silver, gold, and gray spheres represent Pt, *M*, and Zn atoms, respectively. The results of these DFT calculations are in good agreement with those obtained using Matlantis v.7.0.0 (Figure S19), supporting the validity of the large-scale calculations using Matlantis.

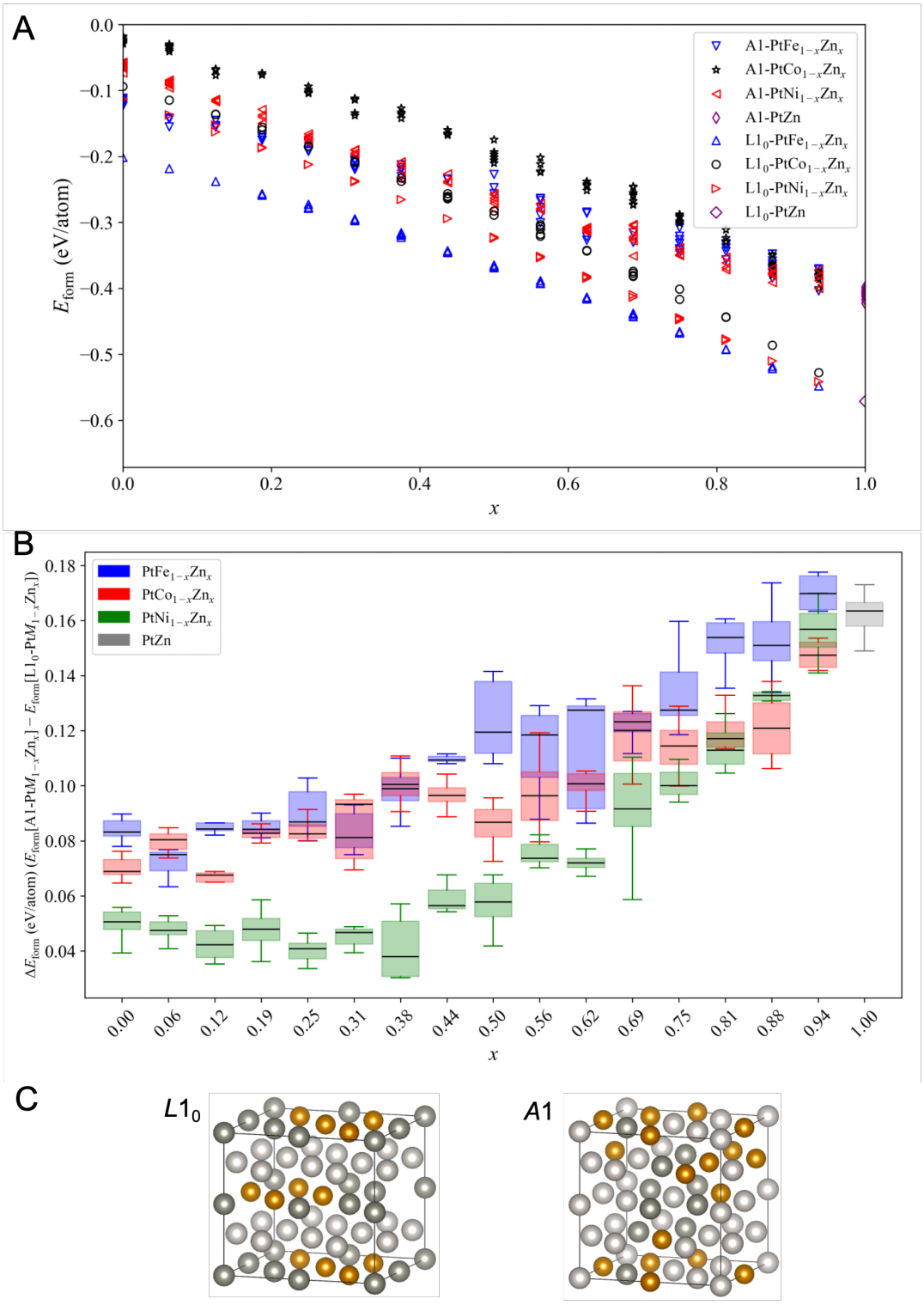

Figure S19. (A) Formation energies (E_{form}) of $A1$-Pt$_1M_{1-x}$Zn$_x$ and $L1_0$-Pt$_1M_{1-x}$Zn$_x$ with varying Zn concentrations (from 0 to 1) calculated using Matlantis v.7.0.0. (B) The difference between E_{form} of the $A1$ and $L1_0$ structures, ΔE_{form}=E_{form}[$A1$-PtM_{1-x}Zn$_x$]–E_{form}[$L1_0$-PtM_{1-x}Zn$_x$]. (C) Examples of structural models of $L1_0$-Pt$_{16}M_{16-x}$Zn$_x$ (left) and $A1$-Pt$_{16}M_{16-x}$Zn$_x$ (right) used for calculations based on neural network potential. Silver, gold and gray spheres represent Pt, M and Zn atoms, respectively.

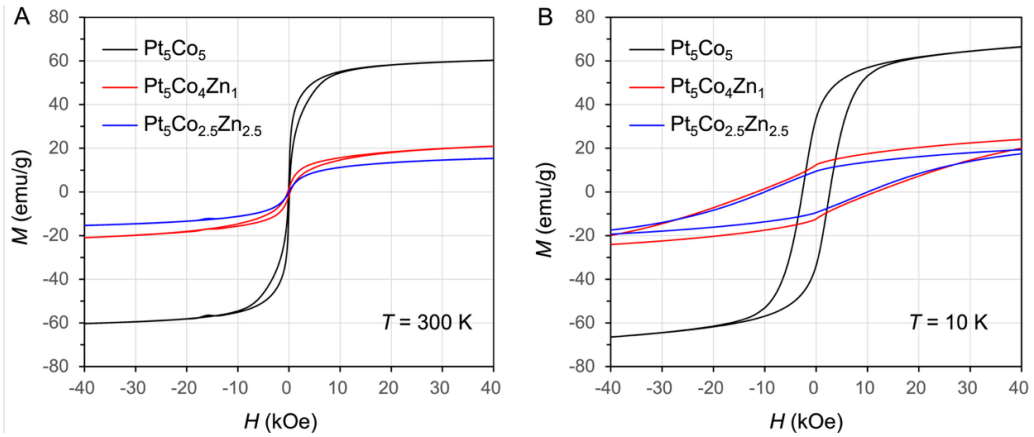

Figure S20. Magnetic hysteresis loops of acid-treated $L1_0$-Pt_5Co_5/C, $L1_0$-$Pt_5Co_4Zn_1$/C and $L1_0$-$Pt_5Co_{2.5}Zn_{2.5}$/C obtained by reductive annealing at 600 °C for 6 h measured at (A) 300 K and (B) 10 K.

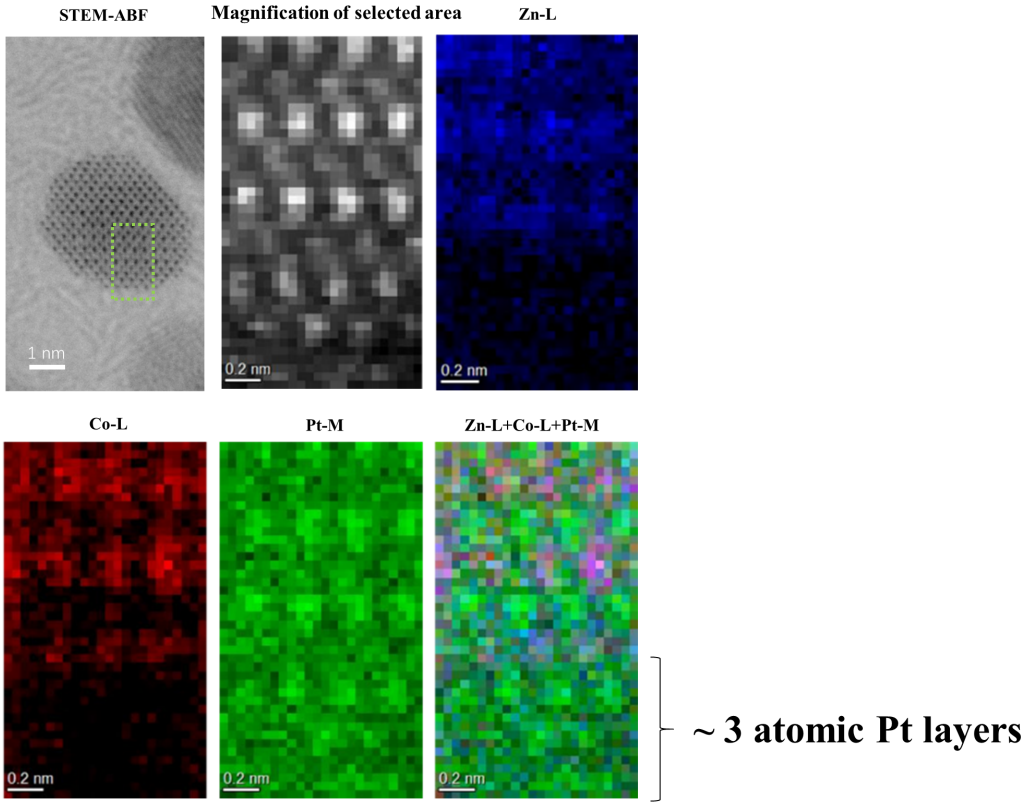

Figure S21. STEM image (top left) and corresponding EELS mapping images showing the approximately three atomic layers of Pt shell at the NP surface of an $L1_0$-$Pt_5Co_{2.5}Zn_{2.5}$@Pt NP.

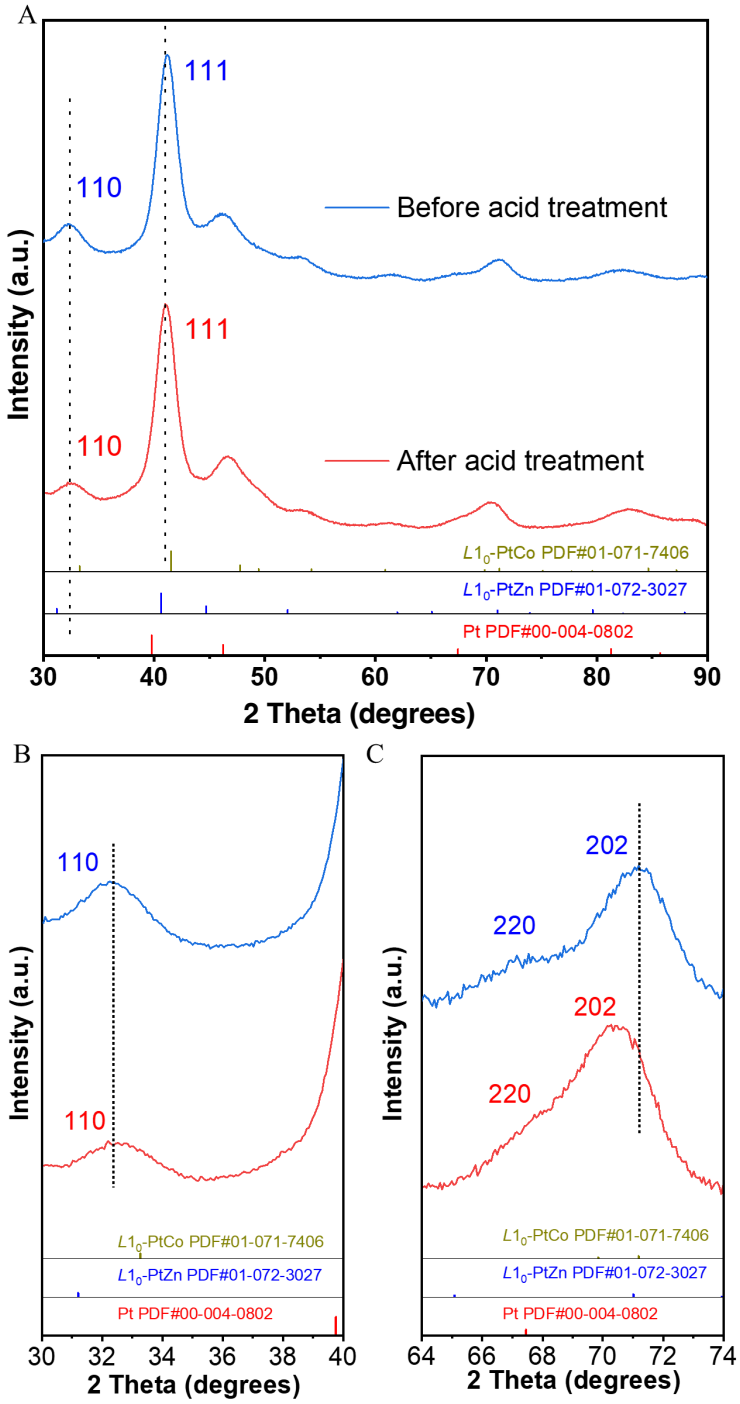

Figure S22. (A) XRD patterns of $L1_0$-$Pt_5Co_{2.5}Zn_{2.5}$/C obtained by reductive annealing at 600 °C for 6 h before and after acid treatment. Magnified views in the ranges between (B) 30° and 40° and (C) 64° and 74°.

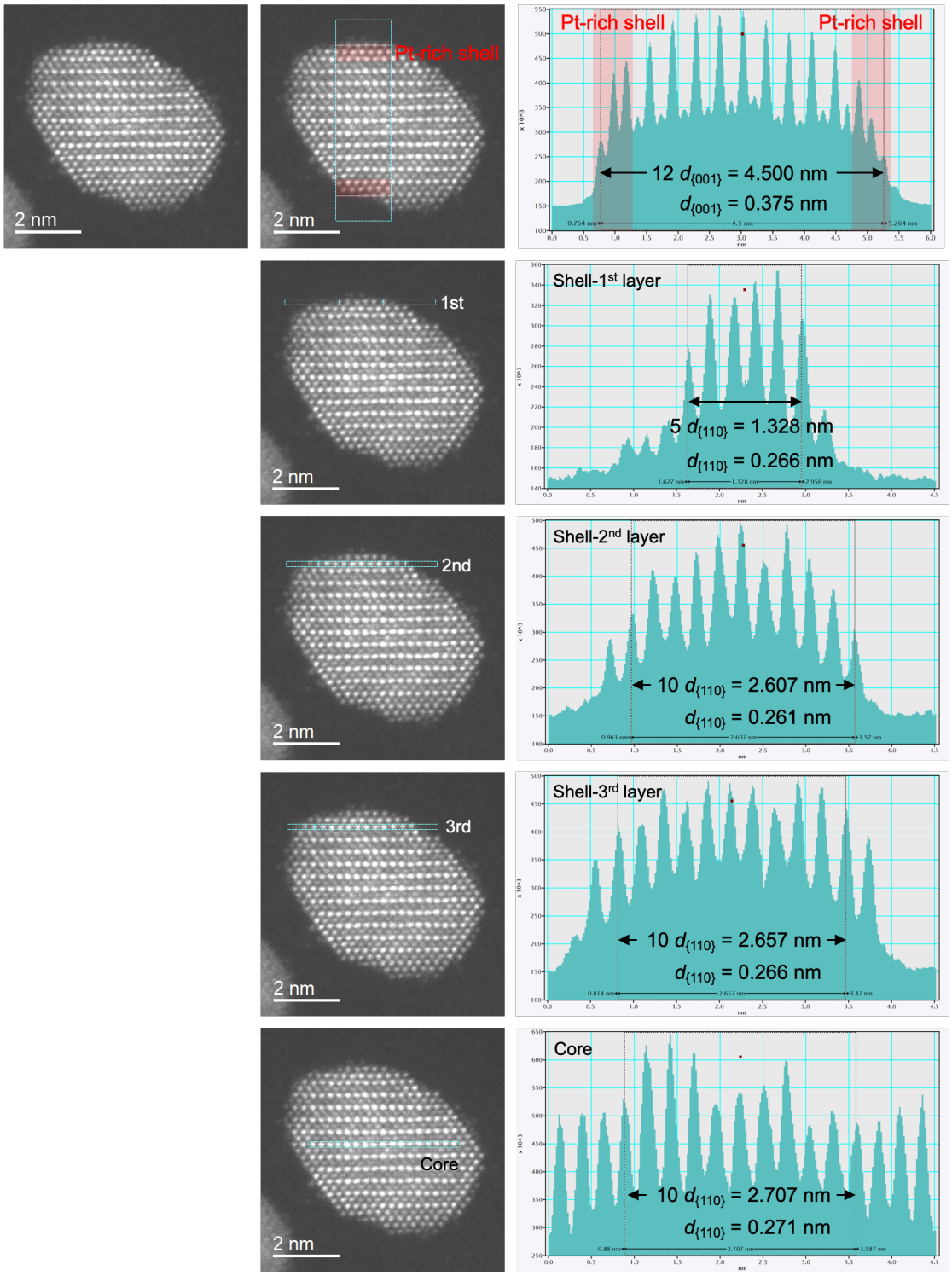

Figure S23. Actual interatomic distances in the {001} planes projected from the <110> direction and the {110} planes projected from the <001> direction in a single $L1_0$-$Pt_5Co_{2.5}Zn_{2.5}$@Pt NP.

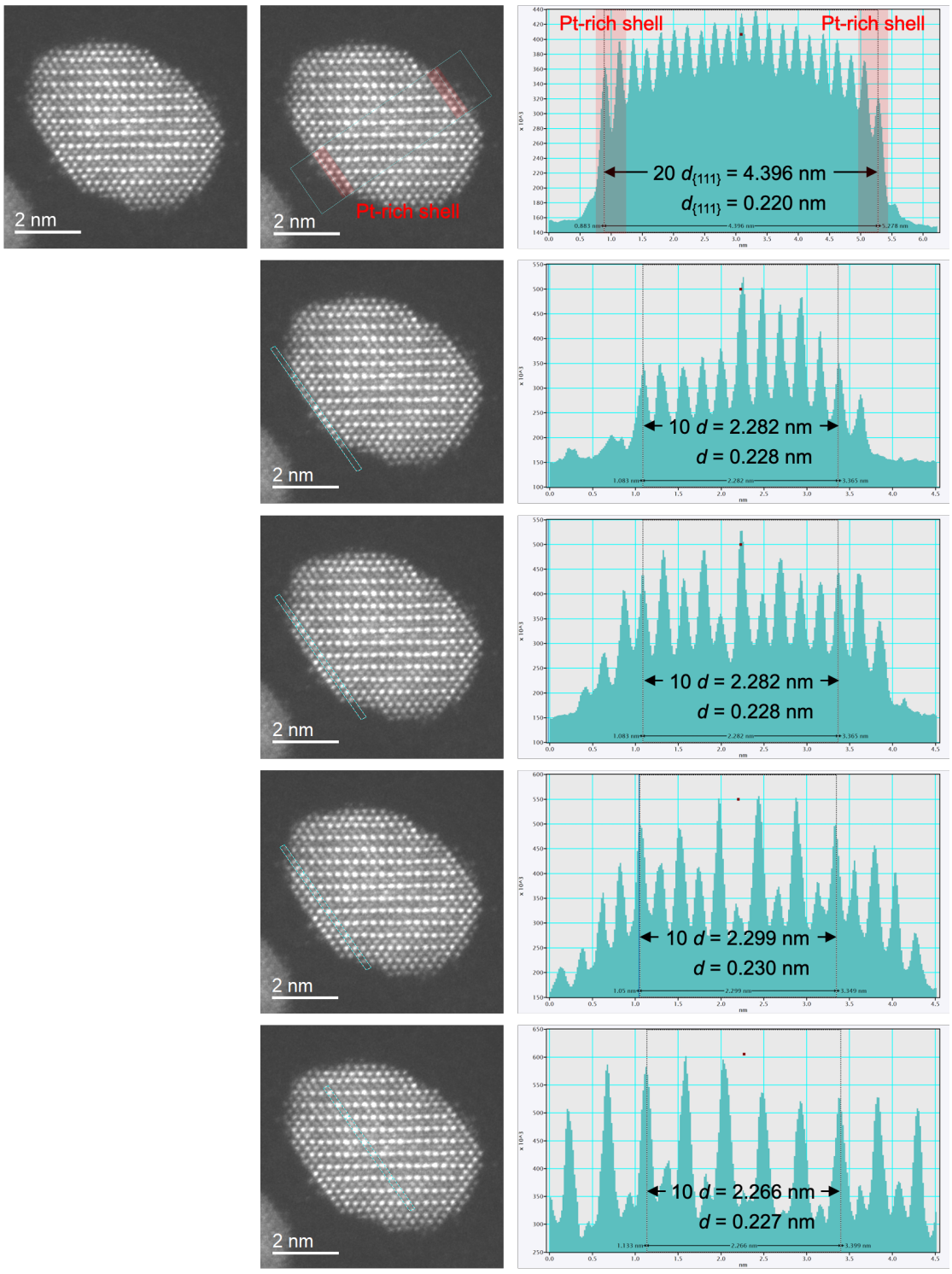

Figure S24. Actual interatomic distances in the {111} planes in a single $L1_0$-$Pt_5Co_{2.5}Zn_{2.5}$@Pt NP.

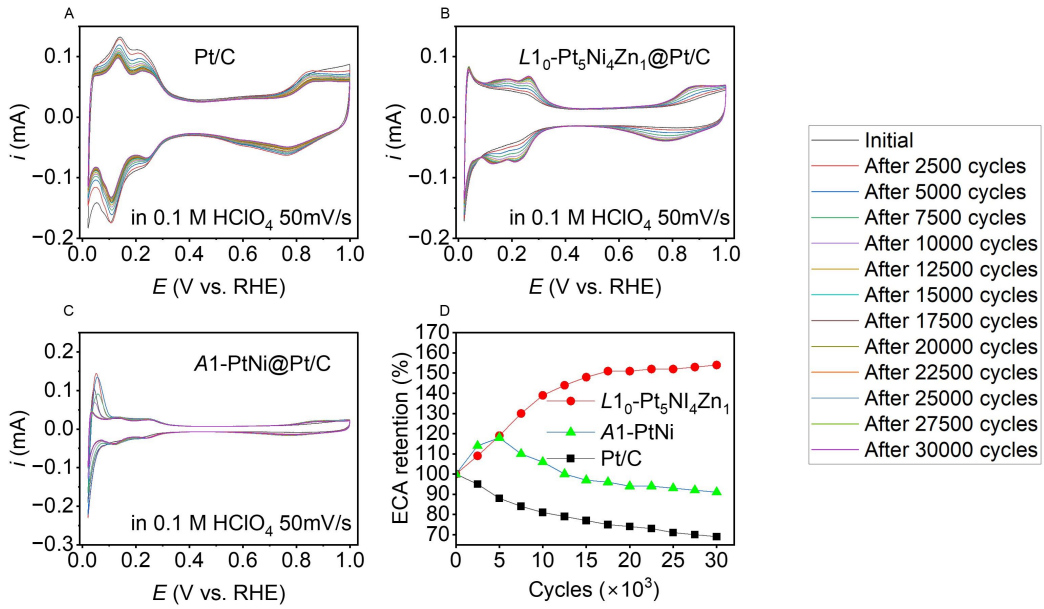

Figure S25. CV measurement for the catalysts (A) commercial Pt/C, (B) $L1_0$-$Pt_5Ni_4Zn_1$@Pt/C and (C) $A1$-Pt_5Ni_5@Pt/C under different ADT cycles. (D) ECSA changing ratio of the prepared catalysts during the ADT cycles in the RDE test.

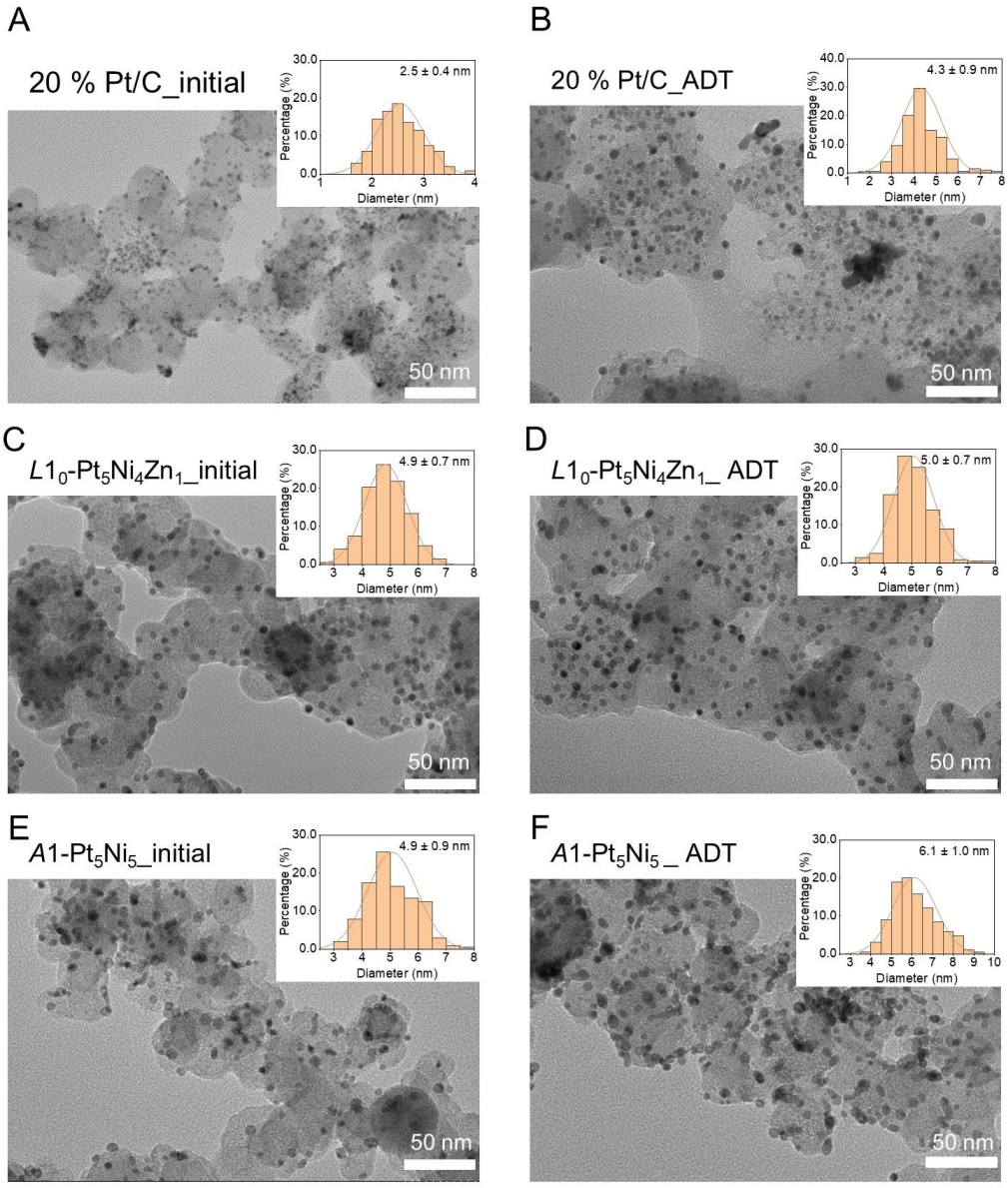

Figure S26. TEM images of (A, B) commercial Pt/C, (C, D) $L1_0$-$Pt_5Ni_4Zn_1$@Pt/C and (E, F) $A1$-Pt_5Ni_5@Pt/C before (A, C, E) and after (B, D, F) ADT cycles.

Supplementary Tables:

Table S1. Literature values of lattice constants of tetragonal ($a = b \neq c$, $\alpha = \beta = \gamma = 90°$) $L1_0$-PtM and cubic ($a = b = c$, $\alpha = \beta = \gamma = 90°$) face-centered cubic (fcc)-Pt.

	Lattice constant				Reference
	$a = b$ (Å)	c (Å)	Volume V (Å^3)	Tetragonality a/c (–)	PDF #
$L1_0$-PtFe	3.852	3.713	55.09	1.037	00-043-1359
$L1_0$-PtCo	3.806	3.684	53.37	1.033	01-071-7406
$L1_0$-PtNi	3.821	3.591	52.43	1.064	01-072-2524
$L1_0$-PtZn	4.050	3.510	57.57	1.154	01-072-3027
cf. fcc-Pt	3.923	3.923	60.37	1	00-004-0802

Table S2. Relative integrated intensities of simulated XRD peaks for fully ordered $L1_0$-Pt(M,Zn) IMCs with various compositions.

Composition	I^*_{110}	I^*_{111}	I^*_{110}/I^*_{111}
$L1_0$-Pt_5Co_5	24.06	100	0.2406
$L1_0$-$Pt_5Co_4Zn_1$	23.30	100	0.2330
$L1_0$-$Pt_5Co_{2.5}Zn_{2.5}$	22.45	100	0.2245
$L1_0$-$Pt_5Co_1Zn_4$	22.14	100	0.2214
$L1_0$-Pt_5Ni_5	22.50	100	0.2250
$L1_0$-$Pt_5Ni_4Zn_1$	22.50	100	0.2250
$L1_0$-$Pt_5Ni_{2.5}Zn_{2.5}$	22.77	100	0.2277
$L1_0$-$Pt_5Ni_1Zn_4$	22.20	100	0.2220
$L1_0$-Pt_5Zn_5	20.99	100	0.2099

Table S3. Average diameters (d_{TEM}) and crystallite sizes (d_{XRD}) of Pt–*M*–Zn NPs before and after reductive annealing obtained from TEM analysis and by applying the Scherrer equation to XRD data, respectively.

Sample	Before annealing	After annealing	
	d_{TEM} (nm)	d_{TEM} (nm)	d_{XRD} (nm)
$Pt_{51}Co_{49}$-650°C	6.5	7.6	6.2
$Pt_{47}Co_{43}Zn_{10}$-600°C	5.4	5.1	4.5
$Pt_{56}Co_{23}Zn_{21}$-600°C	4.8	4.6	4.2
$Pt_{53}Co_{11}Zn_{38}$-550°C	4.2	4.4	4.0
$Pt_{52}Ni_{48}$-10BBA-550°C	6.7	7.1	5.8
$Pt_{52}Ni_{37}Zn_{11}$-550°C	5.2	5.7	4.9
$Pt_{49}Ni_{22}Zn_{29}$-550°C	4.2	4.9	4.6
$Pt_{49}Ni_{9}Zn_{42}$-550°C	3.5	4.8	4.2
$Pt_{53}Zn_{47}$-550°C	2.6	3.7	3.1

Table S4. Compositions and Pt loadings of $L1_0$-Pt(*M*,Zn)/C before and after acid treatment obtained by SEM-EDS and TGA, respectively.

Sample	Composition		Pt loading (%)
	Before acid treatment	After acid treatment	
$L1_0$-Pt_5Co_5-650°C	$Pt_{51}Co_{49}$	$Pt_{56}Co_{44}$	13.8
$L1_0$-$Pt_5Co_4Zn_1$-600°C	$Pt_{47}Co_{43}Zn_{10}$	$Pt_{61}Co_{34}Zn_5$	12.5
$L1_0$-$Pt_5Co_{2.5}Zn_{2.5}$-600°C	$Pt_{56}Co_{23}Zn_{20}$	$Pt_{66}Co_{18}Zn_{16}$	11.2
$L1_0$-$Pt_5Co_1Zn_4$-550°C	$Pt_{53}Co_{11}Zn_{38}$	$Pt_{68}Co_7Zn_{25}$	12.3
$L1_0$-Pt_5Ni_5-550°C	$Pt_{52}Ni_{48}$	$Pt_{57}Ni_{43}$	11.6
$L1_0$-$Pt_5Ni_4Zn_1$-550°C	$Pt_{52}Ni_{37}Zn_{11}$	$Pt_{57}Ni_{34}Zn_9$	12.3
$L1_0$-$Pt_5Ni_{2.5}Zn_{2.5}$-550°C	$Pt_{48}Ni_{22}Zn_{30}$	$Pt_{65}Ni_{14}Zn_{21}$	12.9
$L1_0$-$Pt_5Ni_1Zn_4$-550°C	$Pt_{49}Ni_9Zn_{42}$	$Pt_{62}Ni_8Zn_{30}$	14.3
$L1_0$-Pt_5Zn_5-550°C	$Pt_{53}Zn_{47}$	$Pt_{69}Zn_{31}$	10.9

Table S5. Lattice constants and LRO parameters (S) of $L1_0$-Pt(M,Zn) NPs after reductive annealing determined from Rietveld-refined XRD patterns.

Sample	d_{TEM} (nm)	Lattice constant			I_{110}/I_{111}	LRO parameter S (%)
		$a = b$ (Å)	c (Å)	a/c (–)		
$L1_0$-Pt_5Co_5-650°C	7.6	3.793	3.719	1.020	0.1530	79
$L1_0$-Pt_5Co_5-600°C	6.8	3.797	3.711	1.023	0.1078	65 (low)
$L1_0$-Pt_5Co_5-600°C	5.3	3.806	3.727	1.021	0.0322	37
$L1_0$-$Pt_5Co_4Zn_1$-600°C	5.1	3.815	3.688	1.034	0.1409	78
$L1_0$-$Pt_5Co_{2.5}Zn_{2.5}$-600°C	4.6	3.893	3.678	1.058	0.1473	81
$L1_0$-$Pt_5Co_1Zn_4$-550°C	4.4	3.992	3.528	1.132	0.1226	74
$L1_0$-Pt_5Ni_5-600°C	7.0	3.795	3.749	1.012	0.0255	36
$L1_0$-Pt_5Ni_5-550°C	7.1	3.800	3.702	1.026	0.0494	47
$L1_0$-Pt_5Ni_5-550°C	5.1	3.785	3.695	1.024	0.0406	38
$L1_0$-$Pt_5Ni_4Zn_1$-550°C	5.7	3.844	3.658	1.051	0.1479	81
$L1_0$-$Pt_5Ni_{2.5}Zn_{2.5}$-550°C	4.9	3.961	3.521	1.125	0.1771	88
$L1_0$-$Pt_5Ni_1Zn_4$-550°C	4.8	3.994	3.484	1.146	0.1720	88
$L1_0$-Pt_5Zn_5-550°C	3.7	4.022	3.474	1.158	0.1156	74

Table S6. ECSA values and catalytic activities of $L1_0$-Pt(M,Zn)@Pt/C

Sample	d_{TEM} (nm)	ECSA (m^2_{Pt}/g_{Pt})	Mass activity (A/mg_{Pt})	Specific activity (mA/cm^2_{Pt})
$L1_0$-Pt_5Co_5-650°C	7.6	44	0.752	1.722
$L1_0$-$Pt_5Co_4Zn_1$-600°C	5.1	40	0.686	1.711
$L1_0$-$Pt_5Co_{2.5}Zn_{2.5}$-600°C	4.6	52	0.462	0.881
$L1_0$-$Pt_5Co_1Zn_4$-550°C	4.4	60	0.524	0.876
$L1_0$-Pt_5Ni_5-550°C	7.1	25	0.122	0.491
$L1_0$-$Pt_5Ni_4Zn_1$-550°C	5.2	45	0.629	1.403
$L1_0$-$Pt_5Ni_{2.5}Zn_{2.5}$-550°C	4.9	51	0.643	1.261
$L1_0$-$Pt_5Ni_1Zn_4$-550°C	4.8	42	0.418	0.992
$L1_0$-Pt_5Zn_5-550°C	3.7	60	0.532	0.891
cf. Pt/C	2–3	67	0.205	0.303

Table S7. Surface strain and ORR specific activities of $L1_0$-Pt(M,Zn)@Pt/C

Sample	Lattice constant		{111} triangle area (Å^3)	{111} surface strain (%)	ORR specific activity (mA cm^{-2})
	$a = b$ (Å^3)	c (Å^3)			
Pt_5Co_5-650°C	3.793	3.719	3.074	−7.84	1.722
Pt_5Co_5-600°C	3.797	3.711	3.074	−7.83	n.d.
$Pt_5Co_4Zn_1$-600°C	3.815	3.688	3.081	−7.62	1.711
$Pt_5Co_{2.5}Zn_{2.5}$-550°C	3.893	3.678	3.162	−5.20	0.881
$Pt_5Co_1Zn_4$-550°C	3.992	3.528	3.189	−4.41	0.876
Pt_5Ni_5-550°C	3.800	3.702	3.073	−7.87	0.491
$Pt_5Ni_4Zn_1$-550°C	3.844	3.658	3.098	−7.26	1.403
$Pt_5Ni_{2.5}Zn_{2.5}$-550°C	3.961	3.521	3.149	−5.58	1.261
$Pt_5Ni_1Zn_4$-550°C	3.994	3.484	3.167	−5.05	0.992
Pt_5Zn_5-550°C	4.022	3.474	3.192	−4.30	0.891
Pt (ref)	3.925	3.925	3.335	0	0.303